

# Steady-state thermo-optic model of a continuous-wave Raman laser

Joshua C. Bienfang and Wolfgang Rudolph

*Department of Physics and Astronomy, University of New Mexico, Albuquerque, New Mexico 87131*

Peter A. Roos, Lei S. Meng, and John L. Carlsten

*Department of Physics, Montana State University, Bozeman, Montana 59717*

Received July 2, 2001; revised manuscript received December 6, 2001

We present a model of a cw Raman laser that includes thermo-optic effects that are due to the heating that is inherent in Raman conversion. Thermal lensing and thermal index gratings at high output powers are addressed. With a quadratic duct model we show that broadening of the spatial modes is evident at low Stokes output powers and that accounting for thermal lensing in the laser design can significantly enhance the conversion efficiency. The model agrees with experimental results from a cw H<sub>2</sub> Raman laser and allows for the design of high-power and solid-state cw Raman lasers. © 2002 Optical Society of America  
OCIS codes: 140.3550, 290.5910, 190.4870, 140.6810, 350.6830.

## 1. INTRODUCTION

A Raman-active medium inside a high-finesse optical cavity was recently used to demonstrate cw Stokes generation even when the pump was greatly detuned from one-photon resonance.<sup>1</sup> In such systems the weakness of the off-resonance Raman interaction is overcome with cavity enhancement factors greater than 10<sup>3</sup> for both the pump and the Stokes fields, and it has been shown that a cw Raman laser based on H<sub>2</sub> can reach threshold with less than 1 mW of pump power incident upon the cavity.<sup>2</sup> Because this approach is not restricted to the vicinity of a resonance it can be used to shift a wide variety of pump sources, ranging from the visible to the near infrared, with efficiencies near 66% and thus serves as a useful tool for efficient cw wavelength conversion.<sup>3</sup>

Inasmuch as Raman conversion is a nonparametric process, heating is directly related to the generation of Stokes photons. But, because a typical Raman shift corresponds to a quantum efficiency of 90% or better, heat accounts for a relatively small fraction of the converted pump power, and thermal effects are minimal at low powers. In a recent paper it was shown that below 2 mW of Stokes output the dominant thermal effect is a change in the refractive index at the center of the beams.<sup>4</sup> This change tends to pull the cavity resonance away from the pump frequency and must be compensated for by the locking electronics to maintain a stable output.

In this paper we extend the existing model<sup>2</sup> of the cw Raman laser to include thermal effects, which become more significant at higher Stokes output powers in either gas or solid-state Raman materials. We show that, because of the third-order nature of the Raman interaction, the heat source is sharply peaked at the center of the Gaussian beams. Even at moderate output powers (<100 mW) this heat source sets up a steep index gradient across the fields, which changes the spatial modes in

the cavity. Because both the Raman gain and the coupling efficiency of the pump depend on the spatial modes, these thermo-optic effects are important to the steady-state behavior of the laser. With a quadratic duct model<sup>5</sup> we relate the spatial modes to the circulating powers and show that thermal lensing causes significant deviations from previous laser models. Specifically, we find that thermal lensing causes the spot sizes in the cavity to expand as the Stokes output power increases, which reduces the Stokes power gain and increases the circulating pump power. These effects are investigated experimentally with a cw H<sub>2</sub> Raman laser that is capable of 16 mW of Stokes output, and the model is found to accurately predict the spatial-mode changes and output powers. We also investigate the generation of a thermal index grating in a standing-wave cavity. Losses that are due to a standing-wave thermal index grating in a Raman crystal are predicted to be negligible, in spite of the deleterious thermal properties generally associated with crystals.

In Section 2 we present the steady-state laser model, which includes thermal effects. The spatial modes in the cavity are defined and used to relate the heat source to the circulating powers in the cavity. We then solve the heat diffusion equation to find the temperature throughout the laser cavity. A quadratic fit to the temperature profile is used to model the laser medium as a quadratic duct and to relate the spatial modes to the circulating powers, yielding a set of simultaneous algebraic equations that are solved numerically as a function of the incident pump power. In Section 3 we present experimental results from a cw H<sub>2</sub> Raman laser and show that the thermo-optic model is in good agreement with the observed output powers and spatial-mode changes. In Section 4 we discuss the effects of linear absorption and a thermal index grating in a standing-wave solid-state cw Raman laser.



mirror. We ignore any nonresonant power that couples to higher-order cavity modes. The pump rate is then calculated with the approach of Ref. 2, except that we say that, if  $E_{\text{inc}}$  is the field amplitude incident upon the cavity, then  $a(\xi)E_{\text{inc}}$  is the field amplitude that couples to the cavity mode. Pumping term  $J(\xi)$  is found to be

$$J(\xi) = a(\xi)(T_{1p}P_{\text{inc}}P_p)^{1/2}, \quad (7)$$

where  $T_{1p}$  is the transmissivity at the pump wavelength of the input coupler and  $P_{\text{inc}}$  is the total pump power incident upon the cavity.

The single-pass Stokes power gain  $g(\xi)P_p$  follows from integration of the change in Stokes intensity over the entire cavity. We present this calculation here because it is the foundation of the thermal model below. The change in intensity for the standing-wave Stokes mode  $E_s(r, z, t)$  is<sup>9</sup>

$$\frac{dI_s(r, z)}{dz} = \alpha I_s(r, z)I_p(r, z), \quad (8)$$

where  $\alpha$  is the plane-wave Raman gain coefficient, the intensity is written as  $I_j(r, z) = (n_1/2\eta_0)|\tilde{E}_j(r, z)|^2$ , and  $\eta_0$  is the free-space impedance. The fields are written in terms of their Fourier amplitudes  $\tilde{E}_j(r, z)$ , in cylindrical coordinates, as

$$E_j(r, z, t) = \text{Re}[\tilde{E}_j(r, z)\exp(-i\omega_j t)], \quad (9)$$

$$\tilde{E}_j(r, z) = \frac{2E_j \cos(k_j z)}{\sqrt{1 + \tau^2}} \exp\left[-\frac{r^2}{w_j^2(1 + \tau^2)}\right], \quad (10)$$

where  $z = 0$  occurs at the center of the cavity and  $\tau = 2z/b$ , where  $b = w_j^2 k_j$  is the confocal parameter under the influence of the quadratic duct. We neglect the phase-front curvature and the longitudinal phase shift that occurs as the fields pass through the focal region. Note that these standing-wave fields are written in terms of traveling-wave amplitudes  $E_j$ . In this analysis we neglect the gain asymmetry seen by the copropagating and counterpropagating Stokes fields.<sup>10</sup> Rather, we integrate Eq. (8) over the entire cavity length and divide by 2 to write the change in Stokes power after a single pass down the cavity,  $\Delta P_s$ , as

$$\Delta P_s = g(\xi)P_p P_s, \quad (11)$$

where

$$g(\xi) \equiv \frac{8n_1\alpha}{\lambda_p + \lambda_s} \arctan\left[\frac{l}{b_0\rho(\xi)}\right]. \quad (12)$$

It is worthwhile to note that the single-pass Stokes gain here is twice as large as for the case of a single-pass pump field.<sup>9</sup>

With  $J(\xi)$  and  $g(\xi)$  defined, we solve the steady-state rate equations and obtain the formal solutions

$$P_p = \frac{L_s}{g(\xi)}, \quad (13)$$

$$P_s = \frac{\omega_s}{\omega_p g(\xi)} [a(\xi)(T_{1p}P_{\text{inc}}/P_p)^{1/2} - L_p]. \quad (14)$$

If one were to ignore spatial-mode changes by setting  $\xi = 0$ , these equations would yield the same behavior as

those presented by Brasseur *et al.*<sup>2</sup> To solve Eqs. (13) and (14) we need to relate quadratic index profile  $n(r)$ , and hence the duct parameter  $\xi$  [in Eq. (3)], to the circulating powers  $P_p$  and  $P_s$ .

## B. Thermal Model

The basis of the thermal model is that the energy lost by a pump photon when it is converted to a Stokes photon heats the Raman material. Therefore the heat source in the laser,  $Q(r, z)$  (in watts per cubic centimeter) is proportional to the change in Stokes intensity along the length of the laser. From the conservation condition  $k_p = k_s + \Delta k$  this proportionality is

$$Q(r, z) = \frac{\Delta k}{k_s} \frac{dI_s(r, z)}{dz}, \quad (15)$$

where  $\Delta k$  is the Raman shift,  $k_p$  and  $k_s$  are the pump and the Stokes wave numbers, respectively, and  $dI_s(r, z)/dz$  is given in Eq. (8). For gaseous systems this relationship is complicated by the possibility that the lifetime of the excited vibrational state,  $\tau_{\text{vib}}$ , is not negligible.<sup>4</sup> In this case the random movements of the gas molecules during  $\tau_{\text{vib}}$  distribute the heat over a volume that is larger than that given by  $dI_s(r, z)/dz$  alone. We include this mechanism below. To find the temperature profile in the laser we write the heat source in terms of the circulating powers and then solve the heat equation.

For the  $s \ll 1$  cavity discussed above we take  $\tau^2 \ll 1$  and neglect the expansion of the heat source along the length of the cavity. Also, because of the standing-wave nature of the modes,  $dI_s(r, z)/dz$  oscillates along the cavity length as  $[\cos(k_s z)\cos(k_p z)]^2$ . We therefore split the heat source given by Eq. (15) into two terms:  $Q_0(r)$ , which is independent of  $z$  and is primarily responsible for thermal lensing, and  $Q_{\text{osc}}(r, z)$ , which is an oscillatory term and can set up an index grating along the length of the cavity:

$$\begin{aligned} Q(r, z) &= Q_0(r)[1 + \cos(2k_p z) + \cos(2k_s z) \\ &\quad + \cos(2k_p z)\cos(2k_s z)] \\ &= Q_0(r) + Q_{\text{osc}}(r, z). \end{aligned} \quad (16)$$

The heat equation can be solved separately for each source, and the total temperature distribution is the sum of the two solutions. We note that the characteristic distance<sup>4</sup> traveled by a gas molecule during  $\tau_{\text{vib}}$  is  $(D_g \tau_{\text{vib}})^{1/2}$ , where  $D_g$  is the molecular diffusion constant. For the  $H_2$  laser this distance is of the order of  $10^{-5}$  m, which is 2 orders of magnitude larger than the  $\lambda_j/2$  period of the standing waves. Thus for the  $H_2$  laser the oscillatory heat source term  $Q_{\text{osc}}(r, z)$  is completely washed out by diffusion and does not contribute to the temperature distribution. A partial solution for the longitudinally varying heat source  $Q_{\text{osc}}(r, z)$  is given in Section 4 below and is used to estimate the effect of the resulting index grating on a solid-state Raman laser.

With no molecular diffusion ( $D_g \tau_{\text{vib}} = 0$ ) the heat source  $Q(r, z)$  is given directly by Eq. (15). From Eqs. (8) and (10) one can see that  $Q_0(r) \propto \exp(-r^2/\bar{w}^2)$ , where

$$\frac{1}{\bar{w}^2} = \left( \frac{2}{w_p^2} + \frac{2}{w_s^2} \right). \quad (17)$$

The fact that  $\bar{w}$  is roughly half the size of the field waists is a direct consequence of the third-order nature of the Raman interaction. As in Ref. 4, we include the effects of molecular diffusion during  $\tau_{\text{vib}}$  by modifying  $\bar{w}$  and defining thermal radius  $w_{\text{th}}$  as

$$w_{\text{th}}^2 \equiv \bar{w}^2 \left( 1 + \frac{4D_g \tau_{\text{vib}}}{\bar{w}^2} \right). \quad (18)$$

The total amount of heat deposited in the cell,  $\int d^3r Q(r, z)$ , must be independent of  $\tau_{\text{vib}}$ . With this condition the heat source is found to be

$$Q_0(r) = q_0 \exp\left( -\frac{r^2}{w_{\text{th}}^2} \right), \quad (19)$$

where

$$q_0 \equiv \frac{16\alpha \Delta k}{\pi^2} \frac{P_p P_s}{k_s w_p^2 w_s^2} \left( 1 + \frac{4D_g \tau_{\text{vib}}}{\bar{w}^2} \right)^{-1}. \quad (20)$$

To find the temperature distribution that is due to this heat source we neglect heat flow through the end mirrors and apply Green's function techniques to solve the two-dimensional heat diffusion equation.<sup>11,12</sup> We assume that the cylindrical surface of the Raman medium at radius  $r = R_c$  (the cell walls) is held at its subthreshold temperature  $T_0$ . With this approach it is possible to show that, if the heat source  $Q_0(r)$  turns on at time  $t = 0$ , then the temperature profile is in steady state for times  $t > R_c^2/(4D_T)$  (typically of the order of seconds), where  $D_T$  is the thermal diffusion constant. The steady-state temperature difference  $\Delta T(r) = T(r) - T_0$  is

$$\Delta T(r) = \frac{q_0 w_{\text{th}}^2}{4K_T} \left[ \ln\left( \frac{R_c^2}{w_{\text{th}}^2} \right) - \ln\left( \frac{r^2}{w_{\text{th}}^2} \right) - E_1\left( \frac{r^2}{w_{\text{th}}^2} \right) \right], \quad (21)$$

where  $K_T$  is the thermal conductivity of the Raman medium and  $E_1(x)$  is the exponential integral.<sup>13</sup> This temperature profile is plotted relative to pump waist  $w_p$  in Fig. 2.

As a final step we make a quadratic approximation to the temperature profile. Figure 2 shows that  $\Delta T(r)$  is not well approximated by a parabola: The parabolic fit matches the temperature profile only for  $r/w_p \ll 1$ . However, because the duct model requires a quadratic profile, we make a least-squares parabolic fit over a range  $0 \leq r/w_p \leq r'$ . The value of  $r'$  is somewhat arbitrary, but for  $0 < r' < 2$  the laser behavior is qualitatively identical, with minor quantitative differences. We choose to use the fitting range  $r' = 4/3$ . This range encompasses both  $w_p$  and  $w_s$  and gives good quantitative agreement with experimental data from the  $\text{H}_2$  laser described below. We also require that  $\Delta T(r)$  [Eq. (21)] and the fit have the same value at  $r = 0$ . With this approach we approximate temperature profile  $\Delta T(r)$  with quadratic profile  $\Delta T_{\text{quad}}(r)$ , given by

$$\Delta T_{\text{quad}}(r) = \frac{q_0 w_{\text{th}}^2}{4K_T} \left[ \gamma + \ln\left( \frac{R_c^2}{w_{\text{th}}^2} \right) - (0.518) \frac{r^2}{w_{\text{th}}^2} \right], \quad (22)$$

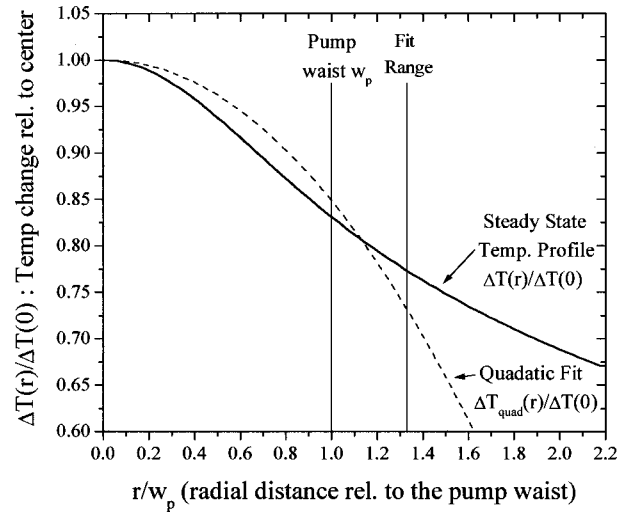


Fig. 2. Steady-state temperature profile  $\Delta T(r)$  and the least-squares quadratic fit from  $0 \leq r/w_p \leq 4/3$ ,  $\Delta T_{\text{quad}}(r)$ .

where  $\gamma$  is the Euler constant ( $\gamma \approx 0.577$ ) and the factor of (0.518) in parentheses is a result of the least-squares fit; with this factor set to unity one retrieves the quadratic expansion of  $\Delta T(r)$ . Quadratic fit  $\Delta T_{\text{quad}}(r)$  is also shown in Fig. 2 and can be seen to approximate the curvature of the temperature profile  $\Delta T(r)$  for  $r/w_p \leq 1$ .

To determine  $n_1$  and  $n_2$ , which define duct parameter  $\xi$  [cf. Eq. (3)], we assume that the index decreases linearly with increasing temperature according to

$$n(r) = n_0 - \left| \frac{\delta n}{\delta T} \right| \Delta T_{\text{quad}}(r), \quad (23)$$

where  $n_0$  is the index at temperature  $T_0$ . Here we have chosen  $\delta n/\delta T$ , the index change per kelvin, to be explicitly negative. For high-pressure gases (as in the  $\text{H}_2$  Raman laser<sup>4</sup>), and for common Raman crystals,  $\delta n/\delta T$  is typically  $\sim -10^{-4} \text{ K}^{-1}$  or smaller.<sup>14</sup> With the temperature profile peaked at the center of the cavity a negative value of  $\delta n/\delta T$  causes the Raman medium to behave as a negative lens, and the waists of cavity modes  $w_j$  will grow wider as increasingly more heat is deposited in the medium. Using  $\Delta T_{\text{quad}}(r)$  from Eq. (22), we find quadratic index profile  $n(r) = n_1 - n_2 r^2$  to be

$$n(r) = n_0 - \left| \frac{\delta n}{\delta T} \right| \frac{q_0 w_{\text{th}}^2}{4K_T} \left[ \gamma + \ln\left( \frac{R_c^2}{w_{\text{th}}^2} \right) \right] + \left[ \left| \frac{\delta n}{\delta T} \right| \frac{(0.518)q_0}{4K_T} \right] r^2. \quad (24)$$

The second term in Eq. (24) gives the change in index at the center of the beams and is of the order of  $10^{-5}$  or smaller for most experimental situations. Although this term is small compared to  $n_0$  it does represent a significant shift in the cavity resonance with respect to the pump frequency.<sup>4</sup> In this steady-state model we assume that the locking electronics account for any shift in the cavity resonance frequency and ignore this term. With this  $n(r)$ , and  $q_0$  from Eq. (20), Eq. (3) is

$$\xi = i \frac{l}{\rho(\xi)} \left\{ \left| \frac{\delta n}{\delta T} \right| \frac{8(0.518)\alpha P_p P_s \Delta k}{\pi^2 n_0 K_T} \frac{1}{k_s w_{0p}^2 w_{0s}^2} \right. \\ \left. \times \left[ 1 + \frac{4D_g \tau_{\text{vib}}}{\rho(\xi)} \left( \frac{2}{w_{0p}^2} + \frac{2}{w_{0s}^2} \right) \right]^{-1} \right\}^{1/2}. \quad (25)$$

This is the duct parameter that we use in the steady-state laser model. Note that, because  $\rho(\xi)$  appears on the right-hand side of Eq. (25), duct parameter  $\xi$  is written as a function of itself. This is an implicit definition of  $\xi$ . An explicit definition of  $\xi$  can be written only if molecular diffusion can be ignored ( $D_g \tau_{\text{vib}} = 0$ ). We present this result in Appendix A. For the H<sub>2</sub> Raman laser we solve Eq. (25) numerically, as discussed below.

### C. Results from the Thermo-Optic Model

With duct parameter  $\xi$  given by Eq. (25) all the terms in the steady state thermo-optic model of the Raman laser are defined. To find the laser behavior for any incident power  $P_{\text{inc}}$  above threshold we solve coupled equations (13), (14), and (25) numerically with the definitions of  $\rho(\xi)$ ,  $\alpha(\xi)$ , and  $g(\xi)$  given above. Figure 3 shows the resultant photon conversion efficiency  $\eta_{\text{ph}}$  as a function of  $P_{\text{inc}}$ , where

$$\eta_{\text{ph}} = \frac{\omega_p (T_{1s} + T_{2s}) P_s}{\omega_s P_{\text{inc}}} \quad (26)$$

and  $T_{1s}$  and  $T_{2s}$  are the transmissivities of the front and the back mirrors, respectively, at the Stokes wavelength. All the laser parameters used to solve the laser equations are from the H<sub>2</sub> laser described in Section 3 below. For comparison we vary the thermo-optic response of the medium  $|\delta n/\delta T|/K_T$  by factors of 2 from four times larger to four times smaller than that of the real H<sub>2</sub> system. We also plot the conversion efficiency when thermo-optic effects are not included in the laser model ( $|\delta n/\delta T|/K_T = 0$ ). From Fig. 3 it can be seen that the peak value of the conversion efficiency is diminished by thermal effects

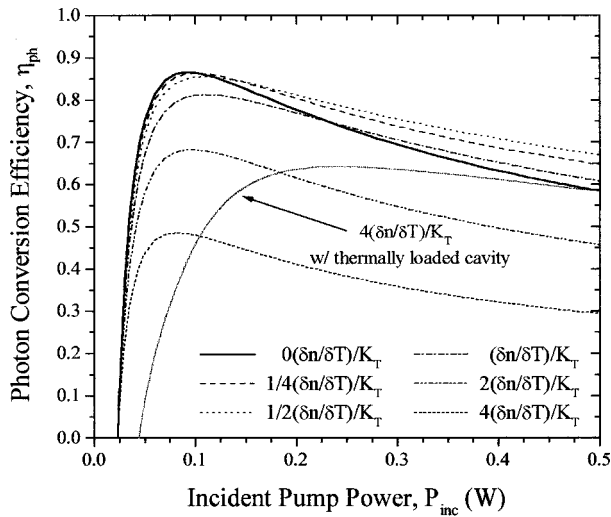


Fig. 3. Photon conversion efficiency versus incident pump power for several thermo-optic responses ( $\delta n/\delta T/K_T$ ) of 10 atm of H<sub>2</sub> gas. Thermally loading the cavity (enlarging the incident pump beam such that optimal coupling requires some thermal lensing) is shown to enhance the efficiency of a laser with a strong thermo-optic response [ $4(\delta n/\delta T)/K_T$ ].

for all values of  $|\delta n/\delta T|/K_T \neq 0$  because of the mismatch of the incident pump and the cavity mode,  $\alpha(\xi)$ . It can be shown that reductions of gain  $g(\xi)$  increase only the incident pump power at which the maximum conversion efficiency is reached, not the maximum conversion efficiency itself. And, because of this fact, we see from Fig. 3 that the conversion efficiency beyond its peak value is actually increased by some values of  $|\delta n/\delta T|/K_T$ . For these cases the conversion efficiency at higher pump powers is enhanced by the lower value of  $g(\xi)$  and is only slightly diminished by decoupling term  $\alpha(\xi)$ . However, for the larger values of  $|\delta n/\delta T|/K_T$  the decoupling term completely overwhelms any enhancement from  $g(\xi)$ , and the conversion efficiency suffers accordingly.

This understanding suggests a simple solution to the decoupling problem. By focusing the incident pump to a waist that is larger than the waist of the cold-cavity mode one can cause the  $\alpha(\xi)$  coupling to increase as the stable cavity mode grows to match the incident-pump mode. This procedure is akin to thermally loading the cavity or to designing the system such that the optimum performance requires a certain amount of thermal lensing. In such a system the laser model is unchanged, except that the pump-coupling term for the thermally loaded (TL) cavity is

$$a^{\text{TL}}(\xi) \equiv \frac{2 \left[ \rho(\xi) \frac{w_{0p}^2}{w_{\text{IN}_p}^2} \right]^{1/2}}{1 + \rho(\xi) (w_{0p}^2/w_{\text{IN}_p}^2)}, \quad (27)$$

where  $w_{\text{IN}_p}$  is the waist of the incident pump mode. In Fig. 3 we show the conversion efficiency of a thermally loaded system for  $4|\delta n/\delta T|/K_T$ , the lowest conversion efficiency. For this plot we set  $w_{\text{IN}_p} = (2.6)w_{0p}$ , and it can be seen that the peak conversion efficiency increased from 48% to 64%. Note that threshold moved to roughly 0.043 W because the incident pump beam is not mode matched to the cold cavity, and thus is not optimally coupled, until there is significant Stokes generation. Increasing  $w_{\text{IN}_p}$  beyond  $(2.6)w_{0p}$  caused the conversion efficiency to decrease. This approach is useful when there is a strong thermo-optic response in the medium. When the thermo-optic response is low (less than that of H<sub>2</sub>) it is more effective to optimize the mirrors.<sup>8</sup>

### 3. EXPERIMENTAL RESULTS

The thermo-optic model presented above was investigated experimentally with a H<sub>2</sub> Raman laser.<sup>3</sup> In this system, pump light is supplied by an injection-locked diode laser that is capable of  $\sim 50$ -mW single-frequency output at 792 nm.<sup>15</sup> This pump is incident upon a high-finesse cavity (HFC) filled with 10 atm of H<sub>2</sub> gas. Subthreshold measurements indicate that  $\sim 74\%$  of the incident pump enters the TEM<sub>0,0</sub> cold-cavity mode. The HFC cavity length is  $l \cong 7.62$  cm, and the radius of curvature of the end mirrors is  $C \cong 50$  cm.

The reflectivities of the HFC mirrors were determined by a combination of transmission and ring-down measurements and found to be  $R_{1p} = 0.99695$ ,  $R_{2p} = 0.99996$ ,  $R_{1s} = 0.99993$ , and  $R_{2s} = 0.99933$ . The absorption in transmission for each mirror was found to be  $A_{1p} = 90$

parts in  $10^6$  (ppm),  $A_{2p} = 15$  ppm,  $A_{1s} = 30$  ppm, and  $A_{2s} = 30$  ppm, with an uncertainty of  $\pm 5$  ppm. We consider  $R_{1p}$  the pump input coupler and  $R_{2s}$  the Stokes output coupler. The vibrational Raman shift in  $H_2$  is  $4155 \text{ cm}^{-1}$ , resulting in Stokes emission at  $1180 \text{ nm}$ . At  $10 \text{ atm}$ , the plane-wave Raman gain is  $\alpha \cong 1.55 \text{ cm/GW}$ ,<sup>16</sup> the thermal conductivity is  $K_T \cong 0.218 \text{ W/(m K}^{-1}\text{)}$ ,<sup>17</sup> the index at room temperature is  $n_0 \cong 1.001269$ ,<sup>18</sup> the index change with temperature is  $\delta n/\delta T \cong -4.30 \times 10^{-6} \text{ K}^{-1}$ , the molecular-diffusion constant<sup>4</sup>  $D_g \cong 0.159 \text{ cm}^2/\text{s}$ , and the lifetime of the excited vibrational state is  $\tau_{\text{vib}} \cong 30 \text{ }\mu\text{s}$ .<sup>19</sup>

We measure the pump beam profile by chopping the transmitted beam and averaging 100 consecutive fall times on a fast digital oscilloscope.<sup>20</sup> This measurement is repeated 10 times for each data point, and the variation of the 10 measurements is used to generate error bars. We find that this technique is most accurate for measuring relative changes in the spot size and does not serve well as an absolute measure of the cavity modes. Thus in Fig. 4 we show the far-field pump spot size relative to its initial value. The filled-circle data points were taken with the HFC tuned outside the Raman gain bandwidth ( $\sim 500 \text{ MHz}$ ), so there is no Stokes generation. Inasmuch as these data points remain close to unity it is clear that changes in the pump spatial mode are not due to thermal effects in the  $H_2$ , mirrors or to coatings as the circulating pump power increases. The open-circle data points were taken with  $10 \text{ atm}$  of  $H_2$  in the HFC and with Stokes light being generated. These data points show that the far-field pump spot size decreases, and hence the waist inside the cavity increases, as more Stokes light is generated. This result is direct evidence that thermal lensing is changing the spatial modes in the cavity. Included in this plot is the theoretical result,  $\rho(\xi)^{-1/2}$  [cf. Eq. (4)], and it can be seen that there is good agreement between theory and experiment.

The pump and Stokes powers measured through mirror  $R_2$  are shown in Fig. 5 relative to incident pump power. In Fig. 5 we also show the results of both the model above and the temperature-independent laser model. It can be seen that, unlike in the temperature-independent model, the circulating pump power does not remain constant as the Stokes output increases. Rather, as the waist inside the cavity increases as shown in Fig. 4, the single-pass gain  $g(\xi)$  decreases. This causes an increase in the circulating pump power [cf. Eq. (13)]. The transmitted pump was measured up to  $50 \text{ mW}$  incident upon the cavity, and within this range there is good qualitative agreement between the model presented here and the performance of the laser. The slight deviation between the model and the pump data at higher powers is most likely due to uncertainties in the transmission coefficient of mirror  $R_2$ . As discussed above, the model was forced to match the Stokes output power data by the appropriate choice of fitting range for the quadratic temperature profile.

#### 4. SOLID-STATE MEDIA

In solid-state Raman media the heat source is not broadened by molecular diffusion. Thus it is necessary to in-

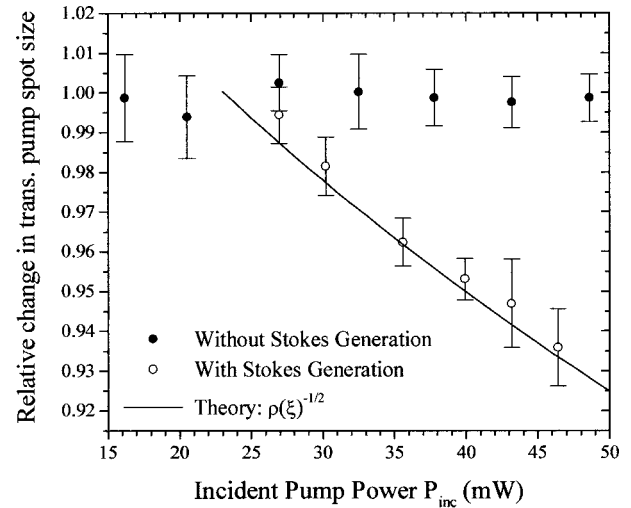


Fig. 4. Pump spot-size measurements outside the cavity relative to its initial value. Data taken without Stokes generation demonstrate the accuracy of the measurement. The decrease in spot size outside the HFC when Stokes light is being generated indicates that the mode inside the HFC is expanding. Results from the theory are also shown.

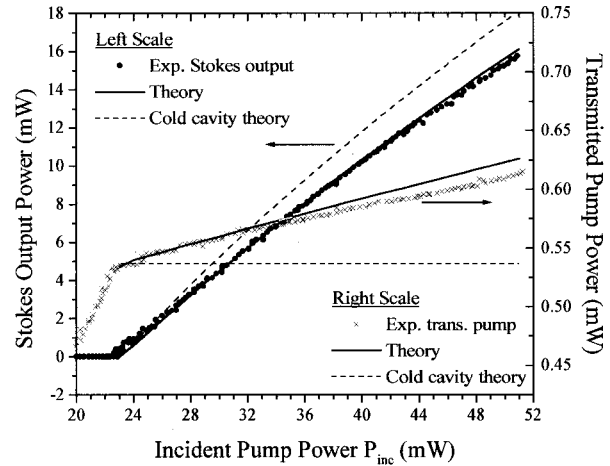


Fig. 5. Transmitted pump and Stokes powers versus incident pump power.

clude the effects of the second heat term,  $Q_{\text{osc}}(r, z)$ , from Eq. (16). This term has oscillatory  $z$  dependence owing to the standing-wave nature of the cavity and therefore acts to create an index grating along the length of the cavity. Such an index grating has the potential to increase the cavity losses through Bragg scattering. Here we investigate the strength of such an effect by solving the heat equation on axis ( $r = 0$ ), where the index grating has the largest amplitude. In this way we establish an upper bound for scattering losses. Also, because most crystals have some linear absorption, we give a brief discussion of such a heat source in the context of the current understanding.

We write the longitudinally varying term in the heat source of Eq. (16) as

$$Q_{\text{osc}}(r, z) = Q_0(r) \sum_{n=1}^4 a_n \cos(2\kappa_n z), \quad (28)$$

where  $Q_0(r)$  is given in Eq. (19) and in the interest of being succinct we have used  $a_1 = a_2 = 1$ ,  $a_3 = a_4 = 1/2$  and  $\kappa_1 = k_p$ ,  $\kappa_2 = k_s$ ,  $\kappa_3 = k_p + k_s$ , and  $\kappa_4 = k_p - k_s$ . We remove the effect of molecular diffusion by setting  $(D_g \tau_{\text{vib}}) = 0$  in Eqs. (18) and (20). To solve the heat equation with this source we use the same Green's function approach used above.<sup>12</sup> Again, we assume that heat source  $Q_{\text{osc}}(r, z)$  turns on at time  $t = 0$ . For this heat source we were able to find an analytic solution only on axis ( $r = 0$ ). Whereas this is an incomplete picture, it is useful for estimating the strength of the index grating because the temperature variation along the  $z$  axis is greatest at the center of the beams. This solution shows that the temperature fluctuations along the beam axis have their steady-state values for times  $t > (\kappa_n^2 D_T)^{-1}$ , where  $D_T$  is the thermal diffusion constant of the Raman medium. For the Raman crystal barium nitrate<sup>15</sup> this time is of the order of picoseconds. Thus we assume that the longitudinal temperature fluctuations are in steady state and find the temperature variation along the beam axis to be

$$T_{\text{osc}}(r = 0, z) = \frac{4\alpha P_p P_s}{\pi^2 K_T w_p^2 w_s^2} \frac{\Delta k}{k_s} \left[ \sum_{n=1}^4 \frac{a_n}{\kappa_n^2} \cos(2\kappa_n z) \right]. \quad (29)$$

This temperature variation causes an index grating that is perfectly Bragg matched to reflect the pump and the Stokes fields. To estimate the diffraction efficiency (at normal incidence) we calculate  $\eta_j = \tanh^2(\pi \Delta n_j d / \lambda_j)$ , where  $\Delta n_j$  is the amplitude of the index grating,  $d$  is the distance traveled in the grating, and  $\lambda_j$  is the free-space wavelength.<sup>21</sup> For the purpose of comparing these scattering losses to the round-trip cavity losses we use  $d = 2l$ . Identifying  $\Delta n_p$  by substituting Eq. (29) into Eq. (23), we find the scattering efficiency for one round trip of the pump to be

$$\eta_p = \tanh^2 \left( \frac{4\alpha P_p P_s}{\pi^2 K_T w_p^2 w_s^2} \frac{\Delta k}{k_s} \frac{l}{n_0 k_p} \left| \frac{\delta n}{\delta T} \right| \right). \quad (30)$$

For barium nitrate, a pump wavelength of  $1 \mu\text{m}$ , and hundreds of watts circulating in the pump and Stokes modes, the scattering efficiency is  $\sim 10^{-10}$ . Because this value is much less than those of the round-trip cavity losses from the mirrors, we do not expect to see any effects as a result of the longitudinal index grating in a standing-wave solid-state Raman cavity.

profiles from  $Q_0(r)$  and  $Q_{\text{osc}}(r, z)$ . As a result of one-photon absorption, this heat source is a Gaussian whose width is  $w \approx 2w_{\text{th}}$ . It follows that the resultant index duct will be roughly half as strong as that of the Raman heat source. Therefore, with the Raman heating equal to the absorptive heating, we still expect the thermal lensing that is due to Raman heating to dominate. This rough sketch may be used to estimate a value for the linear absorption coefficient below which lensing that is due to absorption will be insignificant. We find that for the  $\text{H}_2$  Raman laser described above a power absorption coefficient below  $10^{-5} \text{ cm}^{-1}$  will not cause significant thermal lensing for Stokes output powers above 10 mW. A comparable solid-state system has the same sensitivity.

## 5. CONCLUSIONS

We have presented a steady-state thermo-optic model of a cw Raman laser that includes the effects of thermal lensing and that is in good agreement with experimental results. The applicability of this model is limited primarily by the assumption that  $l \ll C$ . Whereas there is no rule for making the quadratic approximation to the temperature profile, a high degree of accuracy is possible with an appropriate least-squares fit, as shown above. We have addressed the effects of spatial-mode changes on the laser and shown that the performance of a system with a strong thermo-optic response (large  $|\delta n / \delta T| / K_T$ ) can be significantly enhanced by thermal loading of the incident pump mode. We have also addressed some of the issues associated with the use of solid-state Raman materials, including the creation of a standing-wave index grating and heating that is due to linear absorption. Provided that the linear absorption is not large, we find that these complications should not inhibit the performance of such a system. The effects of stress-induced birefringence is an area for further inquiry. The model presented in this paper is useful for predicting the behavior of both gas and solid-state cw Raman lasers at higher Stokes output powers.

## APPENDIX A: WAIST RATIO

With the transfer matrix for a quadratic duct<sup>5</sup> and the laser cavity described above, we find the ratio  $\rho(\xi)$  as defined in Eq. (4) to be

$$\rho(\xi) = \frac{-2}{\sqrt{2s^{-1} - 1}} \left[ \text{Re} \left\{ \xi \left( \frac{(\xi - s^2 \xi^{-1}) \sin(2\xi) + 2s[\cos(2\xi) + \cos(\xi)] - 2s^2 \xi^{-1} \sin(\xi)}{(\xi - s^2 \xi^{-1}) \sin(2\xi) + 2s[\cos(2\xi) - \cos(\xi)] + 2s^2 \xi^{-1} \sin(\xi)} \right)^{1/2} \right\} \right]^{-1}. \quad (\text{A1})$$

Another important consideration for solid-state media is linear absorption. Given the high circulating powers and small spot sizes inside the cw Raman laser cavity, it is conceivable that absorptive heating could be significant. We note that such a heat source has the Gaussian profile of the absorbed beam. The resultant contribution to the temperature profile can therefore be found with the same approach used above and added to the temperature

It can be shown that  $\rho(\xi)$  is real as long as the cavity is stable. The exact value of constant  $\xi_0$  used in Eq. (4) is defined by the condition  $1/\rho(\xi_0) = 0$ . Thus  $\xi_0$  defines the point at which the cavity becomes unstable and is a function of  $s$  alone.

We note that, when the heat source is not broadened by molecular diffusion ( $D_g \tau_{\text{vib}} = 0$ ), the duct parameter  $\xi$  in Eq. (25) can be simplified. In this case we find that the

waist ratio of Eq. (4) can be related directly to the circulating powers as

$$\frac{w_j^2}{w_{0j}^2} = \left[ 1 + \left| \frac{\delta n}{\delta T} \right| \frac{8(0.518)\alpha P_p P_s \Delta k}{\pi^2 n_0 K_T \xi_0^2} \frac{l^2}{k_s w_{0p}^2 w_{0s}^2} \right]^{1/2}. \quad (\text{A2})$$

This expression can be used in the laser equations and also is useful in estimating the circulating powers  $P_s$  for which the cavity is unstable, though it should be noted that, strictly speaking,  $P_p$  and  $P_s$  are not independent quantities.

## ACKNOWLEDGMENTS

This study was supported by the U.S. Air Force Research Laboratories High Power Solid-State Lasers Branch, and by National Science Foundation grant PHYS-9731602.

J. C. Bienfang's e-mail address is bienfang@unm.edu.

## REFERENCES

1. J. K. Brasseur, K. S. Repasky, and J. L. Carlsten, "Continuous-wave Raman laser in H<sub>2</sub>," *Opt. Lett.* **23**, 367–369 (1998).
2. J. K. Brasseur, P. A. Roos, K. S. Repasky, and J. L. Carlsten, "Characterization of a continuous-wave Raman laser in H<sub>2</sub>," *J. Opt. Soc. Am. B* **16**, 1305–1312 (1999).
3. L. S. Meng, P. A. Roos, K. S. Repasky, and J. L. Carlsten, "High conversion efficiency, diode-pumped continuous-wave Raman laser," *Opt. Lett.* **26**, 426–428 (2001).
4. P. A. Roos, J. K. Brasseur, and J. L. Carlsten, "Intensity dependent refractive index in a non-resonant cw Raman laser that is due to thermal heating of the Raman-active gas," *J. Opt. Soc. Am. B* **17**, 758–763 (2000).
5. A. Yariv, *Quantum Electronics*, 3rd ed. (Wiley, New York, 1989), pp. 115–121.
6. L. Casperson and A. Yariv, "The Gaussian mode in optical resonators with a radial gain profile," *Appl. Phys. Lett.* **12**, 355–357 (1968).
7. R. W. P. Drever, J. L. Hall, F. V. Kowalski, J. Hough, G. M. Ford, A. J. Munley, and H. Ward, "Laser phase and frequency stabilization using in optical resonator," *Appl. Phys. B* **31**, 97–105 (1983).
8. K. S. Repasky, L. Meng, J. K. Brasseur, and J. L. Carlsten, "High-efficiency, continuous-wave Raman lasers," *J. Opt. Soc. Am. B* **16**, 717–721 (1999).
9. G. D. Boyd, W. D. Johnston, and I. P. Kaminow, "Optimization of the stimulated Raman scattering threshold," *IEEE J. Quantum Electron.* **QE-5**, 203–206 (1969).
10. Y. S. Choi, "Asymmetry of the forward and backward Raman gain coefficient at 1.54 μm in methane," *Appl. Opt.* **40**, 1925–1930 (2001).
11. J. P. Gordon, R. C. C. Leite, R. S. Moore, P. S. Porto, and J. R. Whinnery, "Long-transient effects in lasers with inserted liquid samples," *J. Appl. Phys.* **36**, 3–8 (1965).
12. H. S. Carslaw and J. C. Jaeger, *Conduction of Heat in Solids*, 2nd ed. (Clarendon, Oxford, 1986), pp. 260–261.
13. M. Abramowitz and I. A. Stegun, eds., *Handbook of Mathematical Functions* (Dover, New York, 1972), pp. 228–229.
14. P. G. Zverev, T. T. Basiev, V. V. Osiko, A. M. Kulkov, V. N. Voitsekhoyskii, and V. E. Yakobson, "Physical, chemical, and optical properties of barium nitrate Raman crystal," *Opt. Mater.* **11**, 315–334 (1999).
15. P. A. Roos, L. S. Meng, J. L. Carlsten, "Using an injection-locked diode laser to pump a cw Raman laser," *IEEE J. Quantum Electron.* **36**, 1280–1283 (2000).
16. J. J. Ottusch and D. A. Rockwell, "Measurements of Raman gain coefficients in hydrogen, deuterium, and methane," *IEEE J. Quantum Electron.* **24**, 2076–2080 (1988).
17. D. E. Gray, ed., *American Institute of Physics Handbook*, 2nd ed. (McGraw-Hill, New York, 1963).
18. D. R. Lide, ed., *Handbook of Chemistry and Physics*, 80th ed. (CRC Press, New York, 1999), p. 6–171.
19. M. M. Audibert, C. Joffrin, and J. Ducuing, "Vibrational relaxation of H<sub>2</sub> in the range 500–40 K," *Chem. Phys. Lett.* **25**, 158–163 (1974).
20. Y. Suzaki and A. Tachibana, "Measurement of the micron-sized radius of Gaussian laser beam using the scanning knife-edge," *Appl. Opt.* **14**, 2809–2810 (1975).
21. H. J. Eichler, P. Gunter, and D. W. Pohl, *Laser-Induced Dynamic Gratings* (Springer-Verlag, Berlin, 1986), pp. 101–107.